ELSEVIER

Chemical Engineering Journal 140 (2008) 43–51

Chemical Engineering Journal

www.elsevier.com/locate/cej

N_2O decomposition over the circulating ashes from coal-fired CFB boilers

Xiangsong Hou *, Hai Zhang, Shi Yang, Junfu Lu, Guangxi Yue

Key Laboratory for Thermal Science and Power Engineering of Ministry of Education, Department of Thermal Engineering, Tsinghua University, Beijing 100084, PR China

Received 16 March 2007; received in revised form 29 July 2007; accepted 30 August 2007

Abstract

The catalytic decomposition of N_2O over the circulating ashes from coal-fired circulating fluidized bed (CFB) boilers was investigated with a fixed bed reactor. The associated kinetics was mimicked by four surrogate metal oxides of SiO_2, Al_2O_3, CaO and Fe_3O_4, which were found as the main components of the circulating ashes. The activation energies and collision coefficients for N_2O thermal decomposition over the circulating ashes and surrogates were individually measured. Experimental results showed that different metal oxides play different roles in the catalytic decomposition of N_2O. Among the components, CaO and Fe_3O_4 are very active, while Al_2O_3 and SiO_2 contribute much less to N_2O destruction. A model based on the specific surface-area-weighted kinetic data of individual surrogates was developed to predict the catalytic decomposition of N_2O over circulating ashes. The predictions agreed with the experimental data with a minor discrepancy acceptable in an engineering view. Some discussions on the discrepancy were given. The O_2 effect on the N_2O decomposition over the circulating ashes was experimentally assessed. It was found that the presence of O_2, even with a small amount, would deteriorate the catalytic decomposition of N_2O.

Keywords: N_2O decomposition; Circulating ashes; Surrogates; Catalytic; CFB boiler

1. Introduction

N_2O (nitrous oxide), an absorber of infrared radiation, is considered as 200–300 times more effective than CO_2 in contribution to global warming through the greenhouse effect. Moreover, since it has the longest lifetimes among the major greenhouse gases, lasting for up to 150 years, N_2O contributes to the stratospheric ozone depletion [1–3].

The furnace temperature in a coal-fired circulating fluidized bed (CFB) boiler is about 1123–1173 K, much lower than that of a pulverized coal-fired boiler, and N_2O formation is more in favor in CFB boilers [4–7]. With the rapid increase of unit number and capacity of CFB boilers around the world, controlling N_2O emission from CFB boilers becomes more and more important.

It was well known that N_2O is thermally instable at a high temperature, and it decomposes as

$$N_2O \rightarrow N_2 + \tfrac{1}{2}O_2 \qquad (A)$$

In a CFB boiler, bed materials interact with N_2O in flue gas in the furnace and the gas–solid separators, e.g., cyclones. These bed materials composing of various kinds of metal oxides could play a catalytic effect on the N_2O destruction and thus accelerate the global decomposition reaction described in Reaction (A) [8–10]. Circulating ashes, the circulating bed materials in the CFB boilers, are generally with narrower size distribution, larger specific area and less carbon content than those bed materials only residing in the furnace and could be excellent catalyst to accelerate N_2O decomposition [9–11]. Interacting with NH_3, the circulating ash can even accelerate the destruction of NO and N_2O at the same time, and thus it was suggested that NH_3 could be added at the cyclone entrance to reduce NO and N_2O emission from CFB boilers [11–13]. Though the importance and effectiveness of the catalytic effect of circulating ash were recognized, the associated chemical kinetics has not been carefully studied.

In general, the circulating ash is a mixture consisting of various metal oxides. Its composition and structure are complex, different among boilers and varied with operation condition for the same boiler. To experimentally determine the chemical kinetics for N_2O decomposition over circulating ashes in such a vast amount of kinds is not trivial. Thus, it is interesting and sig-

* Corresponding author. Tel.: +86 10 62794129 88.
E-mail address: houxiangsong99@mails.tsinghua.edu.cn (H. Xiangsong).

1385-8947/$ – see front matter © 2007 Elsevier B.V. All rights reserved.
doi:10.1016/j.cej.2007.08.033

Nomenclature

Nomenclature

a	cumulative pore area (m^2/g)
A_i	collision coefficient (s^{-1})
c_{N_2O}	N_2O concentration (ppm)
d	pore diameter (Å)
D	inner diameter of reactor (mm)
E	activation energy (kJ mol^{-1})
h	height of bed materials (mm)
h_g	length of the global reacting zone (mm)
k	reaction rate constant (s^{-1})
k_g	global reaction rate constant (s^{-1})
k_i	reaction rate constant over the ith material (s^{-1})
q	reaction rate (ppm s^{-1})
Q	total flow rate of the reacting gases (ml/min)
R_c	universal gas constant (J mol^{-1} K^{-1})
T	temperature (K)
v	reaction order
x_i	mass fraction of the ith component in the circulating ash

Greek letters

ε	porosity of bed materials
τ	time (s)
τ_{bed}	the residence time in bed materials layer (s)

nificant to find out if simple metal oxides can be used as the surrogates for a general description of a circulating ash for N_2O destruction in a CFB boiler.

In this study, the compositions of three different circulating ashes obtained from three different commercial CFB boilers were first measured. Based on the composition measurement and analysis, a few simple metal oxides were selected as the surrogates of the circulating ashes. Then, the kinetic parameters for N_2O destruction over each surrogate and circulating ashes were individually measured. At the same time, a model was developed to describe the overall catalytic effect of circulating ash on N_2O destruction based on each surrogate's kinetic data, mass fraction and specific area fraction in the ash. In last, the discrepancy between the prediction and experimental results was discussed.

2. Experiments

The experiments were conducted on fixed bed reactor system, as shown in Fig. 1.

The fixed bed reactor was the main body of the system and it was made of quartz glass, with an inner diameter of 45 mm and a length of 720 mm. The reactor was placed in an electrically heated tube furnace. Its temperature was well controlled by adjusting the electric voltage on heating elements via a feedback system. A silica distributor plate was sintered in the reactor tube, about 350 mm from the top inlet.

Temperature distribution in the reactor is very important information to study the N_2O decomposition process and the

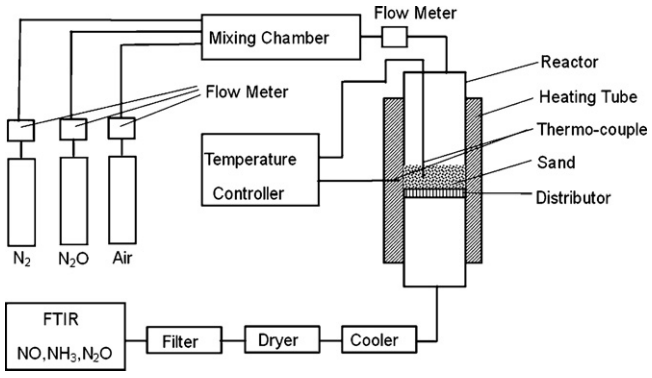

Fig. 1. Schematic of the experimental system.

associated chemical kinetics. Measurements were conducted with a set of thermocouples when the system was in thermal equilibrium. It was found the radial temperature distribution was uniform but the axial temperature profile was in a stage shape, as shown in Fig. 2. The lines in the figure represent calculation results, while the dots are measurement data. It can be seen that there is a flat-temperature zone about 150 mm long, with the maximum temperature, in the middle sector of the reactor. The distributor plate and the bed material over it are located in the flat-temperature zone. Correspondingly, the temperature of the flat zone is the same of the bed material and is often called as the reaction temperature or bed temperature. It should be noticed that the reaction could also happen before and after the flat-temperature zone.

The reacting streams in most cases were gaseous mixtures of N_2O and N_2. Air was introduced into the reacting stream when the influence of O_2 concentration was investigated. Flow rate of each gas was individually measured and controlled by the mass flow meter. The total gas flow rate at the reactor inlet (298 K, 1 atm) in the experiment was kept as $Q = 2500$ ml/min. The gas mixture was introduced into the reactor from the top inlet. After being drought and cleaned, the exhaust gases was detected by a FTIR instrument equipped with a gas cell detector #A10720 VEN 0.2 l/4 m. The measurement accuracy of N_2O was ±5%.

Three kinds of circulating ashes collected from three different CFB boilers were used in the experiment, and they were marked as CA#1, CA#2 and CA#3. In order to avoid involving complex

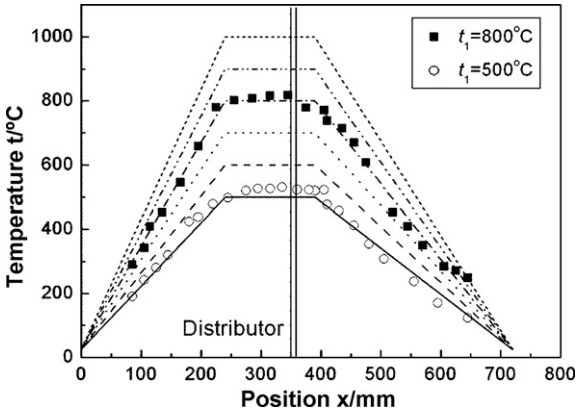

Fig. 2. The axial temperature profiles along the reactor.

mechanisms between N_2O and carbon [7], the bed materials were heated in an electric muffle furnace for 1 h at 1123 K to burn out carbon residues. Bed material with a certain height was evenly placed on the distributor. The porous structure of bed materials was measured by the mercury porosimeter Autopore II 9220 and automatic pycnometers AccPyc 1330.

The residence time of the reacting gases through bed materials, τ_{bed} is:

$$\tau_{bed} = 4.47\frac{\pi D^2 \varepsilon h}{QT} \quad (1)$$

in which, τ_{bed} is the residence time through bed materials layer, in second; D is the inner diameter of the reactor, $D = 45$ mm; ε is the porosity of bed materials. h is the height of bed materials, and during the experiments, $h = 6.29$ mm; Q is the total flow rate of the reacting gases and $Q = 2500$ ml/min in condition of 298 K and ambient pressure; and T is the bed temperature, in K. Obviously τ_{bed} changes with bed temperature and bed material porosity.

3. Results and discussion

3.1. Selection of surrogates

The composition of the circulating ashes was individually measured by an XRD analyzer and the results are shown in Table 1. It can be seen that all three circulating ashes are mainly consisted of oxides of SiO_2, Al_2O_3, Fe_2O_3 and CaO. However, it is worth to point out that the XRD analyzer was only able to detect stable metal oxides.

Consistent with the results of other studies [14,15], SiO_2 is a main composition of the circulating ashes used in the test. In circulating ashes, SiO_2 mainly exist in form of quartz sand or silicate. In present study, highly pure quartz sand was used to represent SiO_2 composition in the circulating ashes.

The Al_2O_3 compound in circulating ashes mainly comes from coal ash or sands in the forms of anorthitte ($CaAl_2SiO_8$), mullite ($Al_6Si_2O_{13}$) and gehlenite ($Ca_2Al_2SiO_7$). Therefore, the analytically pure Al_2O_3 was used to represent Al_2O_3 component in the circulating ashes.

Iron oxide is a very important composition because it is considered as an active catalyst for N_2O decomposition. In ashes of a coal-fired CFB boiler, two kinds of iron oxides, ferric oxide (Fe_2O_3) and magnetite black (Fe_3O_4) possibly exist. It is the temperature and oxygen concentration that decides which kinds of iron oxide is the dominant. It was found that the dominant iron oxide in ashes is Fe_3O_4 instead of Fe_2O_3 and iron oxide enriches on the ash surface [16]. Consequently, Fe_3O_4 was used to represent iron oxide in the circulating ashes, and its mass fraction was calculated from that of Fe_2O_3 listed in Table 1.

$$x_{Fe_3O_4} = \frac{2}{3}\frac{M_{Fe_3O_4}}{M_{Fe_2O_3}} x_{Fe_2O_3} \quad (2)$$

where x is the content of iron oxide in circulating ashes, and $M_{Fe_2O_3}$ and $M_{Fe_3O_4}$ are the mole mass of Fe_2O_3 and Fe_3O_4.

Limestone is often used as the SO_2 sorbent in CFB boilers. Thus, calcium-based compound, mainly in form of limestone ($CaCO_3$), calcined lime (CaO), and sulfated limestone ($CaSO_4$), is often rich in the circulating ashes. CaO was found to be an active catalyst on N_2O thermal decomposition [8,17]. In present study, a limestone, with calcium content of 36.84%, magnesium content of 0.25% was used. The limestone was calcined in an electric muffle furnace at $T = 1123$ K for 1 h.

Based on above discussion, quartz sand and three kinds of simple metal oxide, Al_2O_3, Fe_3O_4 and CaO, were selected as the surrogates for the circulating ashes of CFB boilers.

Fig. 3 shows the distributions of the cumulative pore area for each surrogate measured with the mercury porosimeter. For quartz sand, its cumulative pore area is rather small, 0.049 m^2/g. The cumulative pore area increases sharply with pore diameter d when $d > 5 \times 10^5$ Å, and then gradually increases with further increasing d. The results indicate that the surface of quartz sand is smooth and compact, and the specific surface area is mainly contributed by outer surface of the sand particle rather than the pores. For the Al_2O_3 sample, there are few pores with diameter lager than 500 Å, indicating that the particle surface is smooth. Thus, diffusion through the surface into the inner pores of Al_2O_3 particle for N_2O and the dissociated product molecules is relatively difficult. Shown in Fig. 3, for the Fe_3O_4 and CaO samples, the distributions of the cumulative pore areas are relatively wider and the values corresponding to pore diameter $d > 500$ Å are 0.31 and 4.35 m^2/g, respectively. The surface structure of these two surrogate samples is in favor of gaseous molecule diffusion. Among the four surrogate samples, CaO sample has the largest cumulative pore area for $d \geq 500$ Å.

Table 1
Composition (%) of three circulating ash and quartz sand in weight measured by XRD

	CA#1	CA#2	CA#3	Quartz sand
SiO_2	55.5	64.5	55.7	98.9
$A1_2O_3$	26.3	23.3	36.5	0.8
Fe_2O_3	7.1	6.1	2.4	–
CaO	6.4	2.5	2.4	–
Others	4.7	i.6	3.0	0.3

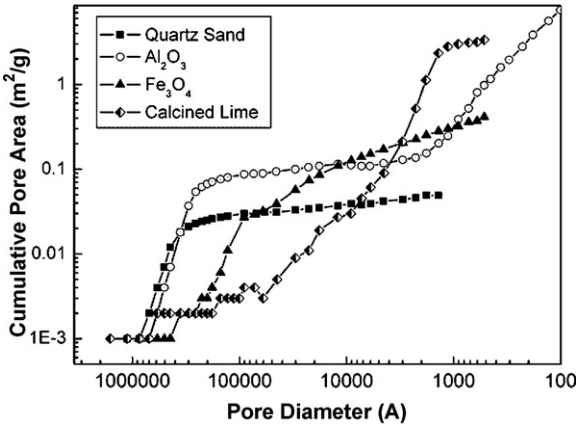

Fig. 3. The distribution of bed material's cumulative pore area with pore diameter.

Table 2
Porosity of the bed materials in experiments

Quartz sand	$A1_2O_3$	Fe_3O_4	CaO	CA#1	CA#2	CA#3
0.47	0.42	0.43	0.40	0.48	0.47	0.43

The porosities of surrogates and circulating ashes were individually measured by automatic pycnometers AccPyc 1330. The measured materials and those used in the reactor were from the same mother samples. The results, given in Table 2, include the internal porosity of the particles. It can be seen that the porosities for all the test samples are nearly the same.

3.2. Kinetic parameters for N_2O decomposition over each surrogate

Fig. 4 depicts the variations of N_2O concentration in the exhaust gas with bed temperature for different bed materials. When Al_2O_3, Fe_3O_4 and CaO were used as bed material, they were mixed with quartz sand in the ratio of 1:9 in mass. For analysis convenience, same experimental conditions were set up for the surrogates as for the circulating ashes. At the reactor inlet, concentration of N_2O in reacting gas stream was kept at about 300 ppm, and total flow rate was kept at 2500 ml/min. The height of the bed material layer was kept at 6.29 mm. It can be seen that compared with the empty reactor, all quartz sand and three metal oxides used as the surrogates of a circulating ash have catalytic effect on N_2O thermal decomposition.

In order to quantitatively describe the catalytic effect of the surrogates, kinetic parameters for the global reaction were derived from the experimental results.

The reaction rate of N_2O thermal decomposition, Reaction (A) is

$$\frac{\mathrm{d}[c_{N_2O}]}{\mathrm{d}\tau} = q_{N_2O} = -k[c_{N_2O}]^v \tag{3}$$

where v is the reaction order.

To obtain the reaction order v in Eq. (3), a series of experiments with inlet N_2O concentrations between 120 and 1100 ppm were conducted at different bed temperatures. The variations of

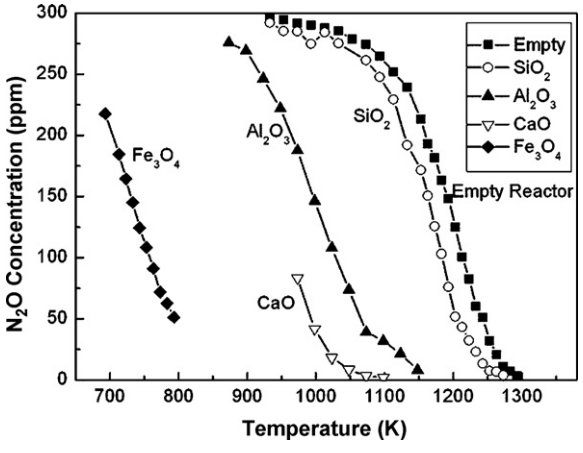

Fig. 4. N_2O concentration in the exhaust gas with/without bed materials ($[O_2]=0$; $[N_2O]_{inlet}=300$ ppm; $Q=2500$ ml/min; $h=6.29$ mm).

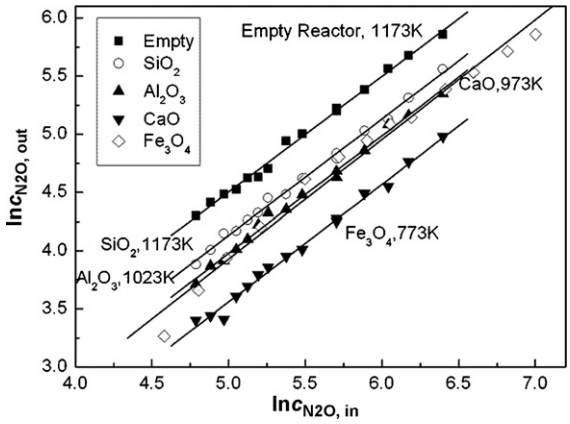

Fig. 5. N_2O concentrations in exhaust gas with different bed materials under different N_2O inlet concentrations ($[O_2]=0$; $Q=2500$ ml/min; $h=6.29$ mm).

logarithmic N_2O concentrations in the exhaust gas $c_{N_2O,out}$ with that in inlet stream $c_{N_2O,in}$ are shown in Fig. 5. The slope of each line represents the reaction order v. The correlation shows, for all kinds of tested bed materials, the reaction order is close to unity, i.e., $v = 1.0$. The result is the same as that for the homogeneous thermal decomposition, which was found to be quite close to a first-order reaction [1,18–20].

However, the reaction mechanisms are different between homogeneous thermal decomposition and heterogeneous one. The former one is determined by the collision of molecules in the gaseous phase, while the later one involves heterogeneous reaction. During the heterogeneous decomposition process, N_2O molecules diffuse to the surface of catalytic particles and then adsorbed by the particles. The adsorbed molecules change their constitution with the charge distribution of the particles. Some adsorbed molecules are activated molecules and rearranged, dissociating into N_2 and O_2, and then departing from the surface of solid particles [2,8,10,21].

Since $v = 1.0$, Eq. (3), can be rewritten and integrated into:

$$\int_{c_{N_2O,1}}^{c_{N_2O,2}} \frac{1}{c_{N_2O}}\,\mathrm{d}c_{N_2O} = \int_0^{\tau} \frac{q_{N_2O}}{c_{N_2O}}\,\mathrm{d}\tau = \int_0^{\tau} -k\,\mathrm{d}\tau \tag{4}$$

then,

$$c_{N_2O,2} = c_{N_2O,1} + \int_0^{\tau} q_{N_2O}\,\mathrm{d}\tau = c_{N_2O,1}\,\exp(-k\tau) \tag{5}$$

Corresponding to the flow path shown in Fig. 6, the reactor is divided into four sections: before-bed section with length of h_1; bed material section with length of h_2; distributor section with length of h_3 and after-distributor section with length of h_4. Homogeneous decomposition can also happen in the before-bed and after-distribution section if temperature is high enough. The overall N_2O decomposition in the reactor is the summation of that in each section, so,

$$\begin{aligned} c_{N_2O,out} = c_5 &= c_{N_2O,in} + \int_0^{\tau_1} q^1_{N_2O}\,\mathrm{d}\tau + \int_0^{\tau_2} q^2_{N_2O}\,\mathrm{d}\tau \\ &\quad + \int_0^{\tau_3} q^3_{N_2O}\,\mathrm{d}\tau + \int_0^{\tau_4} q^4_{N_2O}\,\mathrm{d}\tau \\ &= c_{N_2O,in}\,\exp(-k_1\tau_1 - k_2\tau_2 - k_3\tau_3 - k_4\tau_4) \end{aligned} \tag{6}$$

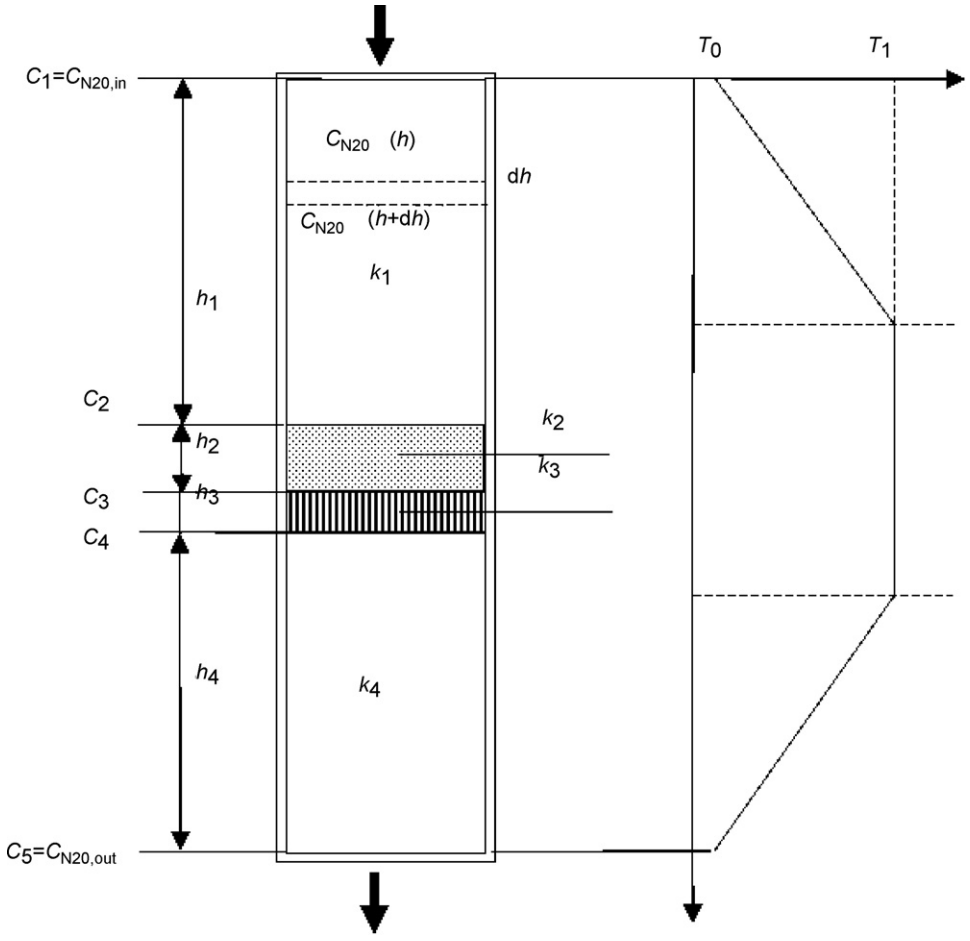

Fig. 6. The N_2O decomposition process along the reactor.

where q_{N_2O} is the reaction rate of N_2O decomposition, ppm s^{-1}, and its superscript denotes the section number; τ is the reaction time in second, and k is the reaction rate constant, and their subscript denotes the section number.

For all tests, N_2O decomposition in before-bed, distributor and after-distributor sections can be regarded as homogeneous thermal decomposition.

$$c_{N_2O,out} = c_{N_2O,in} \exp(-k_1\tau_1 - k_2\tau_2 - k_3\tau_3 - k_4\tau_4) = c_{N_2O,in} x_{homo} \exp(-k_2\tau_2) \quad (7)$$

where $x_{homo} = \exp(-k_1\tau_1 - k_3\tau_3 - k_4\tau_4)$ is a factor related to N_2O decomposition in the entire reactor excluding the bed material section. Obviously, x_{homo} is a function of temperature and the residence time. When the temperature profile and the total flow rate in the reactor are given, x_{homo} and k_2 can be determined by a series of baseline experiments (bed material free in the reactor) with different reaction temperature. For the baseline experiments, k_2 refers to homogeneous decomposition only, namely, $k_2 = k_{homo}(T)$.

When bed material is laid on the distributor, k_2 in Eq. (7) included the homogeneous decomposition and the heterogeneous decomposition as N_2O pass through the bed material layer in time of τ_2. Thus, Eq. (7) can be rewritten as:

$$c_{N_2O,out} = c_{N_2O,in} x_{homo} \exp(-k\tau_2 - k_{homo}\tau_2) \quad (8)$$

After the determination of x_{homo} by baseline experiments, the reaction rate constant of N_2O decomposition over bed material, k can be calculated as:

$$k = \ln\left(\frac{c_{N_2O,in}}{c_{N_2O,out}} \frac{1}{x_{homo}}\right) \frac{1}{\tau_2} - k_{homo} \quad (9)$$

where reaction time, τ_2 in quartz sand layer can be calculated by Eq. (1). Since the bed temperature was rather low in the experiments, it was found that the homogeneous N_2O decomposition only contributed a very small portion to the overall N_2O decomposition. Namely, $k_{homo} \ll k$ and it was negligible for present experiments.

When Al_2O_3, Fe_3O_4 and CaO were tested, no pure samples but mixtures of 10% (in mass) of the sample and 90% (in mass) of the quartz sand were applied. Therefore, the catalytic decomposition of N_2O through the bed material was contributed by the sample and quartz sand. The catalytic decomposition over quartz sand was measured first. When the catalytic decomposition over other surrogates was calculated, both homogeneous decomposition portion along the reactor and quartz sand's catalytic decomposition portion in

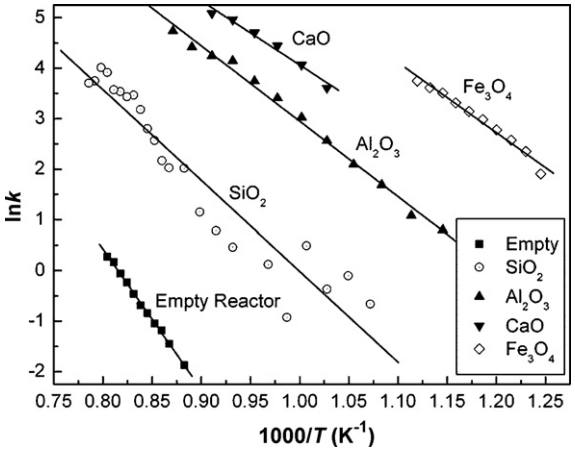

Fig. 7. The reaction rate k with temperature.

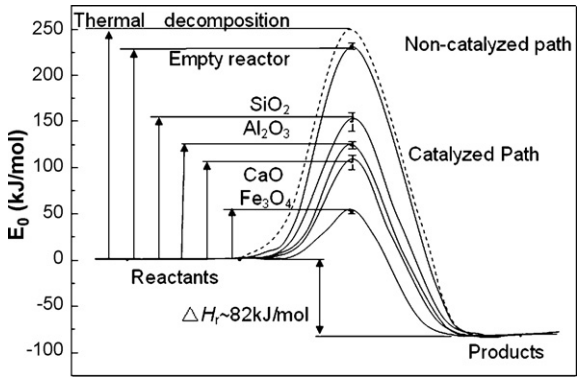

Fig. 8. The activation energy of N_2O thermal decomposition over different metal oxides. The homogeneous one is calculated based on the data of Marinov et al. [18].

bed materials layers were deducted from the overall decomposition.

According to the Arrhenius Theorem, the reaction rate constant k is determined by activation energy E and collision coefficient A

$$k = A \exp\left(\frac{-E}{R_c T}\right) \tag{10}$$

$$\ln k = \ln A - \frac{E}{R_c}\frac{1}{T} \tag{11}$$

The variations of $\ln k$ with $1/T$ for the empty reactor, over quartz sand and three metal oxides are shown in Fig. 7.

Based on Eq. (11), the slope of the lines in Fig. 7 stands for the activation energy E of the N_2O's heterogeneous decomposition, i.e., catalytic decomposition, and E is the intensity indictor of the catalytic effect of the tested sample. The lower the activation energy is, the more active the test sample is. Meanwhile the intercept of the lines with vertical axis is associated with the collision coefficient A_i of the N_2O's heterogeneous decomposition over the bed material, at the tested mass. With the specific surface-area data of each surrogate measured with the mercury porosimeter, the intercept value shown in Fig. 7 can be converted into A_i's based on per unit surface area.

The activation energies E_i and collision coefficient A_i for the unit surface area of the surrogates are given in Table 3.

Fig. 8 shows the changes of internal energy of N_2O molecules during thermal decomposition and the activation energy E_i obtained from Fig. 7, over four surrogates of the circulating ashes and empty reactor. The horizontal ordinate is referred to the conversion of reactants into products, a time scale to describe reaction process. Among the four surrogates, SiO_2 has the largest E_i, indicating that it is not active, while Fe_3O_4 has least E_i and is the most active catalyst for N_2O decomposition. It also can be seen that E_i for empty reactor is nearly the same as that of homogeneous thermal decomposition [18,19], indicating that the reactor's inner surface can be treated as an inert surface.

The effect of the amount of bed material on the kinetics of N_2O decomposition was investigated with different heights of bed material. The experiments showed that kinetic parameters were insensitive to the amount of bed material, and thus they can be determined with a given height of bed material.

3.3. Mimic of catalytic decomposition over circulating ashes with surrogates

The overall catalytic effect of the circulating ash is the synergetic effect of every active component on its surface. For a specific component, the collision coefficient A_i is in direct proportion with its surface area. Assuming that the all components are well mixed in circulating ash, the surface area for each component should be the product of its mass fraction and the specific area of the circulating ash. Thus, the reaction rate constant for N_2O decomposition over a circulating ash, k_{CA} can be calculated as:

$$k_{CA} = \sum_i \frac{a_{CA} x_i}{a_i} A_i \exp\left(\frac{E_i}{R_c T}\right) \tag{12}$$

where i refers to species of SiO_2, Al_2O_3, CaO and Fe_3O_4 and x_i is the mass fraction of the ith component in the circulating ash. a denotes the specific surface area, m^2/g. A_i and E_i are respectively the collision coefficient and activation energy of for N_2O decomposition over the ith component as we discussed

Table 3
The chemical kinetics parameters for the surrogates

Surrogates	Activation energy (kJ mol^{-1})	Collision coefficient (s^{-1})	Collision coefficient for the unit area of surrogates (s^{-1} m^{-2})
SiO_2	149.25	6.202×10^7	9.04×10^7
$A1_2O_3$	123.95	5.743×10^7	3.25×10^7
CaO	105.53	1.904×10^7	0.40×10^7
Fe_3O_4	52.15	1.698×10^7	2.83×10^7

Table 4
The specific surface area of the test sample ($d \geq 5000$ Å)

Test sample	SiO_3	$A1_2O_3$	CaO	Fe_2O_3	CA#1	CA#2	CA#3
Specific surface area (m^2/g)	0.049	0.263	4.35	0.311	0.6475	0.500	0.538

in last section. For each sample, the specific surface area was derived by the data measured by the mercury porosimeter for pore diameter $d \geq 500$ Å, shown in Table 4.

Given the catalytic decomposition reaction is of the first order, the concentration of N_2O in exhaust gas, expressed in Eq. (8) can be rewritten as:

$$c_{N_2O,out} = c_{N_2O,in} x_{homo} \exp(-k_{CA}\tau_2 - k_{homo}\tau_2) \quad (13)$$

where k_{CA} is the reaction rate constant of heterogeneous N_2O destruction over the circulating ash calculated by Eq. (12); τ_2 is the residence time in circulating ash layer, other symbols are defined in Eq. (8).

By using above model, the N_2O concentrations in the exhaust gas for a given bed temperature, inlet N_2O concentration and flow rate were predicted. The model predictions and experimental results are compared in Fig. 9. The dots represent the results by experiments, while the lines stand for the results by model prediction with Eq. (13). It can be seen that the model predictions and experimental results agree well. The model slightly underestimates N_2O destruction for CA#1 and CA#2 in high temperature region, and overestimates N_2O destruction for CA#1 in low temperature region.

It was suspected that the cross-effect between surrogates was one of the reasons to cause the discrepancy. Thus, three artificial ashes were composed by the surrogates in the mass fraction analogues to the circulating ashes listed in Table 1, and marked as CA#1′, CA#2′ and CA#3′. Similar experiments were repeated for these artificial ashes. The variations of N_2O concentration in exhaust gas with the bed temperature for the artificial ashes are shown in Fig. 10. Also in this figure, the results predicted are

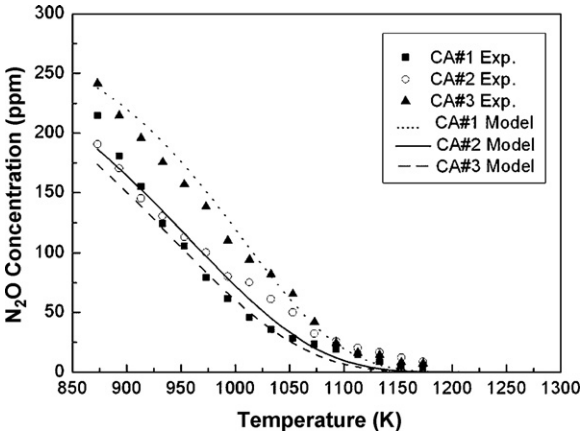

Fig. 9. The catalytic decomposition of N_2O over circulating ashes obtained by experiment and model prediction ($[O_2] = 0$; $[N_2O]_{inlet} = 300$ ppm; $Q = 2500$ ml/min; $h = 6.29$ mm).

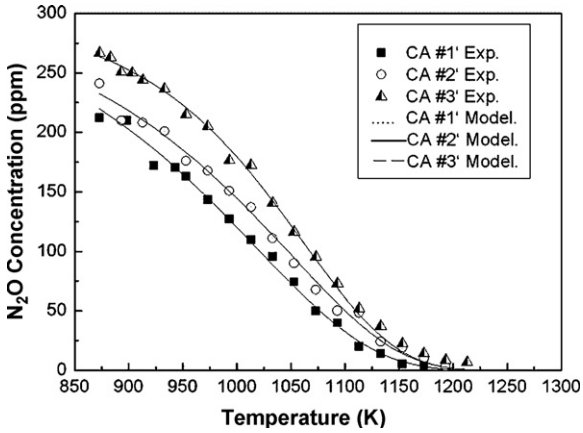

Fig. 10. The catalytic decomposition of N_2O over the mixture of surrogates and model prediction ($[O_2] = 0$; $[N_2O]_{inlet} = 300$ ppm; $Q = 2500$ ml/min; $h = 6.29$ mm).

given. The reaction rate constant $k_{CA'}$ is calculated as

$$k_{CA} = \sum_i x_i A_i \exp\left(\frac{E_i}{R_c T}\right) \quad (14)$$

The results predicted by as Eqs. (14) and (13), in which no cross-effect is considered.

It can be seen that the experimental data and corresponding model prediction agree with each other very well. The discrepancy is within the experimental error. This result indicates that the cross-effect between the surrogates is inappreciable.

The main cause to the discrepancy we believed was that only four main compositions of the circulating ash were considered. In this study, only the metal oxides with mass fractions over 1% were taken into account and used as a surrogate. Some other active metal oxides such as MgO and CuO were neglected, even though they were detected. It was found that these metal oxides even in a small amount in weight, might have appreciable catalytic effect on N_2O decomposition [8,22,23].

Another reason for the discrepancy might be due to the difference of surface crystal structure between the circulating ashes and the surrogates in which the distribution of each metal oxide is regarded as uniform. In addition, the discrepancy may be partially attributed to the difference in cumulative pore area between the surrogates and circulating ashes.

Nevertheless, the discrepancy between the model prediction and experiments for the three circulating ashes is within a relative value of ±20% or an absolute value of 10 ppm. In an engineering view, the prediction is of acceptable accuracy. Of course, more experiments are recommended to validate the correctness of the model.

4. N_2O formation and destruction in CFB boilers

Besides the catalytic decomposition of N_2O over the circulating ashes discussed above, it would be of significance to discuss the overall N_2O formation and destruction in a CFB boiler.

The N_2O formation mechanisms include the homogenous oxidation of hydrogen cyanide, heterogeneous oxidation of fixed nitrogen in char residue and reduction of NO with char or

CO [24–26]. About 10–50% of the volatile cyan and cyanide compounds of the fuel nitrogen, such as HCN, are oxidized homogeneously to N_2O. The main reaction path from hydrogen cyanide to N_2O is

$$HCN \xrightarrow{O} NCO \xrightarrow{NO} N_2O \quad (B)$$

Additionally, part of N_2O, counting for 1–20% of the total N_2O amount, is generation by Reaction (C) by the reaction between NO and char-N, the nitrogen residue in the char after devolatilization. It could be an important path of N_2O formation from char-N, depending on fuel type and pyrolysis conditions [24–26].

$$(–CN) + NO \rightarrow N_2O + (–C) \quad (C)$$

In the furnace, both homogeneous decomposition and heterogeneous decomposition of N_2O occur. Both carbon or char particles and circulating ashes play catalytic effect on N_2O decomposition. Nevertheless, N_2O formation rate is larger than the destruction rate, so the concentration of N_2O increases with height of furnace [17,27]. It was also found that the flue gas composition such as CO_2, H_2O, O_2, CO and SO_2 are also important for N_2O homogeneous reaction [27].

In this study, the O_2 effect was experimentally assessed. The results, shown in Fig. 11, illustrate that when 1.0% of O_2 is added into the reacting gas stream, the N_2O reduction over the circulating ashes is remarkably weakened. For example, at the bed temperature of 1123 K, the N_2O conversion drops from more than 90% to about 50%.

The influence of O_2 concentration on catalytic decomposition is caused by the selective adsorption of the particles surface. When O_2 is present, O_2 atoms will occupy some active locations on circulating ash surface. As a result, the adsorption of N_2O decreases.

It was well known that increasing the temperature of furnace or cyclone separator can accelerate the catalytic decomposition rate of N_2O. Though it is an effective approach for the removal of N_2O from CFB boilers, such an approach is limited by desulphurization, slagging and increase of NO formation.

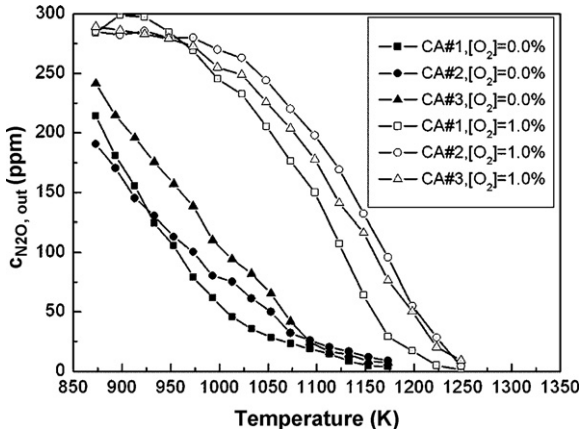

Fig. 11. Catalytic decomposition of N_2O with O_2 ($[N_2O]_{inlet} = 300$ ppm; $Q = 2500$ ml/min; $h = 6.29$ mm).

5. Conclusions

The circulating ashes from coal-fired CFB boilers were found mainly made up of SiO_2, Al_2O_3, CaO and Fe_3O_4. Consequently, four analytically pure samples of these metal oxides were used as the surrogates for the circulating ashes on catalytic decomposition of N_2O.

Experiments were conducted in a fixed bed reactor with well-controlled temperature profile. The activation energy and collision coefficient, and the catalytic effect for N_2O destruction over each surrogate and the circulating ashes were measured. It was found that CaO and Fe_3O_4 are the most important component in the ashes for N_2O destruction.

A model was proposed to predict the overall decomposition rate of N_2O over circulating ashes using the kinetic data of individual surrogates weighted by their specific surface-area fraction in the circulating. The predictions agreed well with the experimental data, within a relative value of ±20% or an absolute value of 10 ppm. Some discussions on the discrepancy were given, and cross-effect between surrogates was excluded.

Besides the catalytic effect of circulating ashes, N_2O formation and destruction in a CFB boiler also depends on the coal type, bed temperature, product gases such as H_2O and CO_2, and excess air. The O_2 effect on the N_2O decomposition over the circulating ashes was experimentally assessed. The results showed that the presence of O_2, even with a small amount, could deteriorate the catalytic decomposition of N_2O over the circulating ash. More detail experimental studies with further consideration of these influences are suggested.

Acknowledgments

The financial supports by Chinese National Program on Key Basic Research (2006CB200301) and Chinese Nature Science Foundation (50406002) are gratefully acknowledged.

References

[1] H. Liu, B.M. Gibbs, Modeling of NO and N_2O emissions from biomass-fired circulating fluidized bed combustors, Fuel 81 (2002) 271–280.
[2] L. Armesto, H. Boerrigter, H. Bahillo, J. Otero, N_2O emission from fluidized bed combustion. The effect of fuel characteristics and operating conductions, Fuel 82 (2003) 1845–1850.
[3] R.A. Brown, L. Muzio, N_2O Emissions from fluidized bed combustion, in: Proceedings of the 11th International Conference on Fluidized Bed Combustion, 1991.
[4] B.X. Shen, T. Mi, D.C. Liu, B. Feng, Q. Yao, F. Winter, N_2O emission under fluidized bed combustion condition, Fuel Process. Technol. 84 (2003) 13–21.
[5] H. Zhang, J.F. Lu, K.Y. Chen, H.R. Yang, G.X. Yue, An experimental study on N_2O reduction over circulating ashes of CFB boilers, in: Proceedings of the 18th International Conference on Fluidized Bed Combustion, Toronto, Canada, 2005.
[6] X.S. Hou, G.X. Yue, H. Zhang, J.F. Lu, H.R. Yang, Reduction of N_2O and NO by NH_3 on circulating ashes: the effect of oxygen concentration, in: 19th International Fluidized Bed Combustion Conference, Vienna, Austria, 2006.
[7] Y. Zhao, H. Lu, Y. He, J. Ding, L. Yin, Numerical prediction of combustion of carbon particle clusters in a circulating fluidized bed riser, Chem. Eng. J. 118 (2006) 1–10.

[8] P.F.B. Hansen, K. Dam-Johanen, J.E. Johnsson, T. Hulgaard, Catalytic reduction of NO and N_2O on limestone during sulfur capture under fluidized bed combustion conditions, Chem. Eng. Sci. 47 (1992) 2419–2424.
[9] X.S. Hou, J.P. Li, H. Zhang, S.T. Zhao, J.F. Lu, G.X. Yue, Limestone effects on NO_x formation in CFB combustors, in: The Fifth PR China–Korea Joint Workshop on Clean Energy Technology, Qingdao, China, 2004.
[10] A.N. Hayhurst, A.D. Lawrence, The reduction of the nitrogen oxides NO and N_2O to molecular nitrogen in the presence of iron, its oxides, and carbon monoxide in a hot fluidized bed, Combust. Flame 110 (1997) 351–365.
[11] H. Zhang, J.F. Lu, K.Y. Chen, H.R. Yang, G.X. Yue, An experimental study on N_2O reduction over circulating ashes of CFB boilers, in: Proceeding of the 18th International Conference on Fluidized Bed Combustion, Toronto, Canada, 2005.
[12] X.S. Hou, H. Zhang, G.X. Yue, Feasibility study on NO_x reduction by coke oven gas reburning, in: The Sixth Korea–China Joint Workshop on Clean Energy Technology, Busan, Republic of Korea, 2006.
[13] D. Fissore, R. Pisano, A.A. Barresi, Observer design for the selective catalytic reduction of NO_x in a loop reactor, Chem. Eng. J. 128 (2007) 181–189.
[14] H. Maenami, N. Isu, E.H. Ishida, T. Mitsuda, Electron microscopy and phase analysis of fly ash from pressurized fluidized bed combustion, Cem. Concr. Res. 34 (2004) 781–788.
[15] I. Demir, R.E. Hughes, P.J. DeMaris, Formation and use of coal combustion residues from three types of power plants burning Illinois coals, Fuel 80 (2001) 1659–1673.
[16] Y.T. Yuan, Q. Yang, L.Q. Qi, Study on the characteristics of fly ash from CFB, Boiler Technol. 37 (2003) 29–32 (in Chinese).
[17] J.E. Johnsson, Formation and reduction of nitrogen oxides in fluidized-bed combustion, Fuel 73 (1994) 1398–1415.
[18] N.M. Marinov, W.J. Pitz, C.K. Westbrook, M. Hori, N. Mastsunaga, An experimental and kinetic calculation of the promotion effect of hydrocarbons on the NO–NO_2 conversion in a flow reactor, Proc. Combust. Inst. 27 (1998) 389–396.
[19] P. Glarborg, M.U. Alzueta, K. Dam-Johansen, J.A. Miller, Kinetic modeling of hydrocarbon/nitric oxide interactions in a flow reactor, Combust. Flame 115 (1998) 1–27.
[20] G. Löffler, D. Andahazy, C. Wartha, F. Winter, H. Hofbauer, NO_x and N_2O formation mechanisms—a detailed chemical kinetic modeling study on a single fuel particle in a stationary fluidized bed, in: 16th International Conference on Fluidized Bed Combustion Reno, Nevada, 2001.
[21] G. Löffler, V.J. Wargadalam, F. Winter, H. Hofbauer, Decomposition of nitrous oxide at medium temperature, Combust. Flame 120 (2000) 427–438.
[22] V. Barišic, A.K. Neyestanaki, F. Klingstedt, P. Kilpinen, K. Eränen, M. Hupa, Catalytic decomposition of N_2O over the bed material from circulating fluidized-bed (CFB) boilers burning biomass fuels and wastes, Energy Fuels (2004) 1909–1920.
[23] P. Glarborg, J.E. Johnsson, K. Dam-Johanen, Kinetics of homogeneous nitrous oxide decomposition, Combust. Flame 99 (1994) 523–532.
[24] G.X. Yue, F.J. Pereira, A.F. Sarofim, J.M. Beér, Char nitrogen conversion to NO_x in a fluidized bed, Combust. Sci. Technol. 83 (1992) 245–256.
[25] W. Ren, X.B. Xiao, J.F. Lu, G.X. Yue, Research on conversion of nitrogen in char during combustion under fluidized bed conditions, J. China Univ. Min. Technol. 32 (2003) 259–262 (in Chinese).
[26] A. Molina, E.G. Eddings, D.W. Pershing, A.F. Sarofim, Char nitrogen conversion: implication to emissions from coal-fired utility boilers, Progr. Energy Combust. Sci. 26 (2000) 507–531.
[27] L.A.C. Tarelho, M.A.A. Matos, J.M.A. Pereira, Influence of limestone addition on the behaviour of NO and N_2O during fluidised bed coal combustion, Fuel 85 (2006) 967–977.